Robotica (2009) volume 27, pp. 1063–1073. © Cambridge University Press 2009
doi:10.1017/S0263574709005487

Biped gait generation based on parametric excitation by knee-joint actuation

Yuji Harata*†, Fumihiko Asano‡, Zhi-Wei Luo§, Kouichi Taji† and Yoji Uno†

†*Department of Mechanical Science and Engineering, Graduate School of Engineering, Nagoya University, Furocho, Chikusa, Nagoya 464-8603, Japan*
‡*School of Information Science, Japan Advanced Institute of Science and Technology, 1-1 Asahidai, Nomi, Ishikawa 923-1292, Japan*
§*Department of Computer and Systems Engineering, Graduate School of Engineering, Kobe University, 1-1 Rokkodai, Nada, Kobe 657-8501, Japan*

(Received in Final Form: February 10, 2009. First published online: March 17, 2009)

SUMMARY
Restoration of mechanical energy dissipating on impact at the ground is necessary for sustainable gait generation. Parametric excitation is one approach to restore the mechanical energy. Asano *et al*. ("Parametric excitation mechanisms for dynamic bipedal walking," *IEEE International Conference on Robotics and Automation* (2005) pp. 611–617.) applied parametric excitation to a biped robot with telescopic-legs, in which up-and-down motion restores total mechanical energy like playing on the swing. In this paper, parametric excitation principle is applied to a kneed biped robot with only knee actuation and it is shown that the robot walks successively without hip actuation. We also examine influences of several parameters and reference trajectory on walking performance.

KEYWORDS: Biped gait; Dynamic walking; Parametric excitation; Energy restoration; Knee-joint actuation.

1. Introduction

Passive dynamic walking proposed by McGeer [1] has received much attention because of the higher energy efficient gait generation method. In passive dynamic walking, a biped robot walks continuously and stably down the slope by gravity with no mechanical input. The kinetic energy lost by the collision at the ground is restored by transporting potential energy to kinetic energy in descending an incline. However, on the level ground the energy restoration by gravity is impossible. Therefore, it is necessary to restore the kinetic energy by certain mechanical input, such as ankle torque, hip torque and so on. A so-called virtual passive dynamic walking proposed by Asano *et al*. [2] and energy tracking control proposed by Goswami *et al*. [3] are examples of methods that make passive dynamic walking possible on level ground.

Another approach for restoring kinetic energy is parametric excitation which is a principle to increase the amplitude of vibration by swinging. Asano *et al*. [4] applied the parametric excitation method to a biped robot with a telescopical actuator in its legs. They showed that energy restoration was realized by elongating and contracting the swing-leg. Asano *et al*. [5] also applied this method to a real robot. The telescopic-legs have another advantage in that the elongating and contracting swing-leg resolves the problem of scuffing the ground.

In this paper, we apply the parametric excitation method to a kneed biped robot. When a biped robot bends and stretches its knees to avoid scuffing the ground, the center of mass of a swing-leg moves up and down similar to a telescopic-leg, and hence, mechanical energy is expected to be restored by parametric excitation. Based on this observation, we propose the gait generation method in which the mechanical energy lost by the collision is restored by bending and stretching a knee adequately.

We first verify that the total mechanical energy of a biped robot increases by the motion of a double pendulum which is very similar to a swing-leg. We then show that a sustainable gait can be generated by this approach in numerical simulations. In this method, we use only knee torque. We have already proposed parametric excitation based walking for a kneed biped robot and have shown that the robot can walk sustainably.[6] But there have been two deficiencies. One is the problem of foot clearance when a robot scuffs the ground, and another is that there is a singular posture for which the input knee torque cannot be calculated. In this paper, we resolve the above two problems. For the former, we resolve the foot clearance problem by means of revising the ratio of the thigh and shin lengths. For the latter, we resolve it by giving a reference trajectory to the relative angle of a knee. In ref. [6] the reference trajectory is defined as the distance between the hip joint and the center of mass of the swing-leg. We also introduce the bending delay which defines the starting time of bending a knee and is used to optimize the reference trajectory (see Section 5.1).

This paper is organized as follows: Section 2 describes a biped robot with semicircular feet. Section 3 explains the parametric excitation principle and its application to a biped robot with telescopic-legs. In Section 4, we show that

* Corresponding author. E-mail: y_harata@nuem.nagoya-u.ac.jp

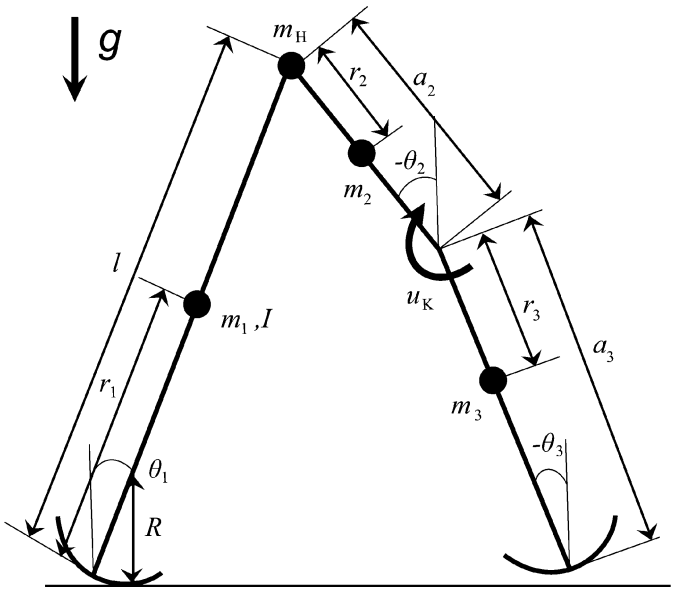

Fig. 1. Model of planar kneed biped robot with semicircular feet.

knee bending and stretching restores mechanical energy by a double pendulum. Section 5 is the main part of this paper, in which we apply parametric excitation to a biped robot with knees. Section 6 discusses the effect of parameters and the basin of attraction. Finally, in Section 7, we conclude the paper.

2. Model of Planar Kneed Biped Robot with Semicircular Feet

Figure 1 illustrates the biped robot dealt with in this paper. The robot has four point mass and three degrees of freedom, and has semicircular feet whose centers are on each leg. Since there are two mass on the leg, the support-leg has an inertia moment. The dynamic equation during single support phase is given by

$$\boldsymbol{M}(\boldsymbol{\theta})\ddot{\boldsymbol{\theta}} + \boldsymbol{C}(\boldsymbol{\theta}, \dot{\boldsymbol{\theta}})\dot{\boldsymbol{\theta}} + \boldsymbol{g}(\boldsymbol{\theta}) = \boldsymbol{S}u_K - \boldsymbol{J}^{\mathrm{T}}\lambda, \qquad (1)$$

where $\boldsymbol{\theta} = [\theta_1\ \theta_2\ \theta_3\ ]^{\mathrm{T}}$ is the generalized coordinate vector, $\boldsymbol{M} \in \mathbb{R}^{3\times3}$ is the inertia matrix, $\boldsymbol{C} \in \mathbb{R}^{3\times3}$ is the Coriolis force and the centrifugal force, $\boldsymbol{g} \in \mathbb{R}^3$ is the gravity vector, and $\boldsymbol{S}u_K$ is the control input vector. These are described in detail in Appendix A. The matrix $\boldsymbol{J} = [0 \quad 1 \quad -1\,]$ is the Jacobian derived from a knee constraint, $\dot{\theta}_2 = \dot{\theta}_3$, and $\lambda \in \mathbb{R}$ is the knee binding force. In this robot, collisions occur at the knee and the ground. Therefore, the robot has three phases:

- The first phase (Single support phase I): The support-leg rotates around the contact point between a semicircular foot and the ground, and the swing-leg is bent.
- The second phase (Single support phase II): The support-leg rotates around the contact point like in phase I, but the knee of the swing-leg is locked in a straight posture. When the first phase changes to the second phase, a collision occurs at the knee.
- The third phase (Double support phase): This phase occurs instantaneously, and the support-leg and the swing-leg are exchanged after the collision at the ground.

When a swing-leg straightens, a completely inelastic collision is assumed to occur at a knee of the swing-leg. We also assume that, once after collision, a knee-joint is fixed by the force $\boldsymbol{J}^{\mathrm{T}}\lambda$ until collision at the ground. Impact equations are described in Appendix B.

3. Parametric Excitation

Parametric excitation is a phenomenon in which the amplitude of vibration increases by swinging itself. Figure 2 presents the optimal trajectory, A→B→C→D→E, given by Lavrovskii and Formalskii,[7] along which the increase of total mechanical energy is maximized, supposing that the length of a pendulum, l, is changed instantaneously. However, the length cannot be actually changed instantaneously, and hence a reference trajectory close to the optimal trajectory is chosen to restore total mechanical energy. Asano *et al.* [4] applied the parametric excitation principle to a biped robot with telescopic-legs by pumping the swing-leg mass. The

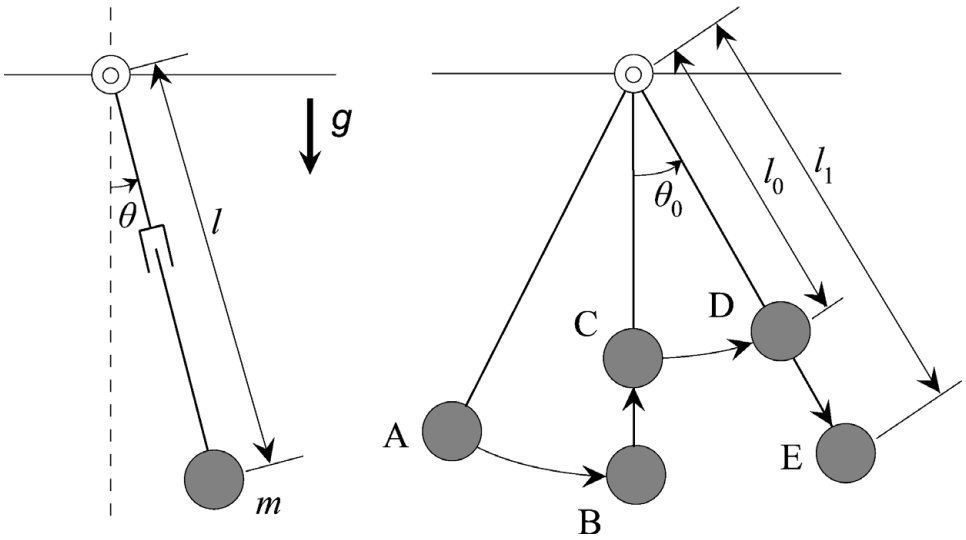

Fig. 2. Optimal trajectory of pendulum in parametric excitation.

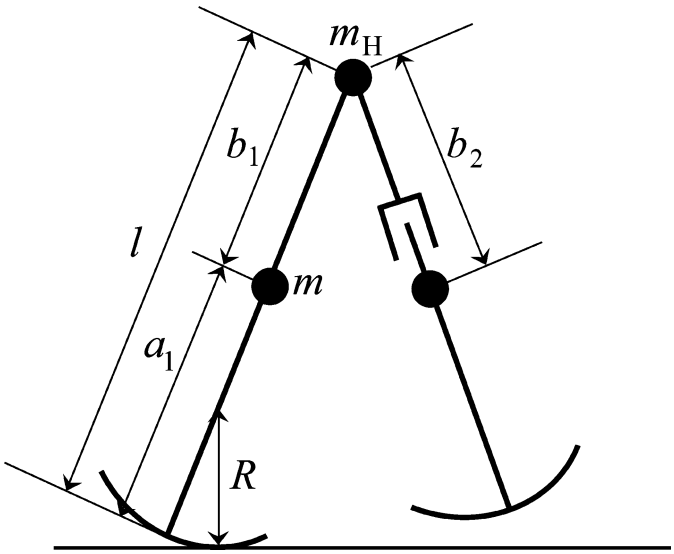

Fig. 3. Three-link model of a planar underactuated biped robot with telescopic-legs.

telescopic-leg length, b_2, in Fig. 3 is controlled to track the reference trajectory. Instance just after the collision at the ground is set as $t = 0$, and the reference trajectory, $b_{2d}(t)$, is given by

$$b_{2d} = \begin{cases} b_1 - A_m \sin^3\left(\frac{\pi}{T_{\rm set}} t\right) & (t \le T_{\rm set}) \\ b_1 & (t > T_{\rm set}), \end{cases} \tag{2}$$

where b_1 is the distance between hip and mass point when the telescopic-leg is straightened, A_m is the desired amplitude of vibration, and $T_{\rm set}$ is the desired settling-time which is assumed before heel-strike collisions. In other words, the condition $T \ge T_{\rm set}$ must hold for the steady-step period T. We call this the settling-time condition. Figure 4 shows the simulation result of parametrically excited dynamic bipedal walking by swing-leg actuation.

Remark 3.1. *The optimal trajectory shown in Fig. 2 has nothing but theoretical meaning because the center of mass cannot be moved instantaneously in real machines. Moreover, there is significant difference between a pendulum and the biped robots in Figs. 1 and 3 in that the hip joint of a biped robot is movable while the supporting point of a pendulum is fixed at a ceiling, and hence the trajectory in Fig. 2 may not be optimal for biped robots. In spite of this, we will adopt the reference trajectory of the control input close to the trajectory of Fig. 2 with the expectation of increasing kinematic energy. As shown later (Section 5.1), a reference trajectory is completely tracked by the proposed control method when the trajectory is sufficiently smooth.*

Table I. Physical parameters of kneed biped robot in Fig. 1.

r_1	0.40	m	R	0.5	m
r_2	0.20	m	m_1	5.0	kg
r_3	0.30	m	m_2	1.0	kg
a_2	0.40	m	m_3	4.0	kg
a_3	0.60	m	m_H	5.5	kg
l	1.00	m	I	0.20	kg · m^2

4. Parametric Excitation of Double Pendulum

It was shown [4] that total mechanical energy of a biped robot with telescopic-legs was restored by the parametric excitation approach. We verify that total mechanical energy of a biped robot with knees can also increase by the parametric excitation approach. A double pendulum, of which only the joint between two links is actuated, mimics a kneed-actuation leg. We note that the pendulum does not strike the ground, but a collision at a joint occurs like a biped robot when a joint is straightened. The dashed line in Fig. 5 illustrates a virtual telescopic pendulum which connects a support point and center of mass of the pendulum. This virtual telescopic pendulum is controlled to track the reference trajectory. For simplicity, the reference trajectory is given for a relative angle by

$$(\theta_2 - \theta_3)_d = \begin{cases} A_m \sin^3\left(\frac{\pi}{T_{set}} t\right) & (t \le T_{\rm set}), \\ 0 & (t > T_{\rm set}). \end{cases} \tag{3}$$

The joint is actuated during only the first half of cycle. We set $t = 0$ as instance of $\theta_2 = \theta_3 > 0$ and $\dot\theta_2 = \dot\theta_3 = 0$. Figures 6–8 show the results of numerical simulation. The parameters of the double pendulum are shown in Table I (Section 5). The total mechanical energy is shown in Fig. 6. Figure 7 is the enlarged illustration of Fig. 6, and Fig. 8 shows the distance between a support point and the center of mass of the pendulum. Figure 6 shows that total mechanical energy increases during one cycle. It is observed from Figs. 7 and 8 that the total mechanical energy increases when bending and decreases when straightening. We have assumed that the collision at a joint occurs, but mechanical energy is not

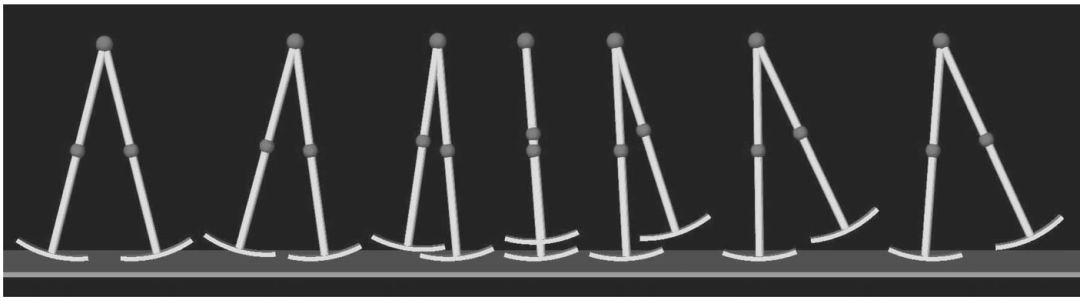

Fig. 4. Parametrically excited dynamic bipedal walking by swing-leg actuation.

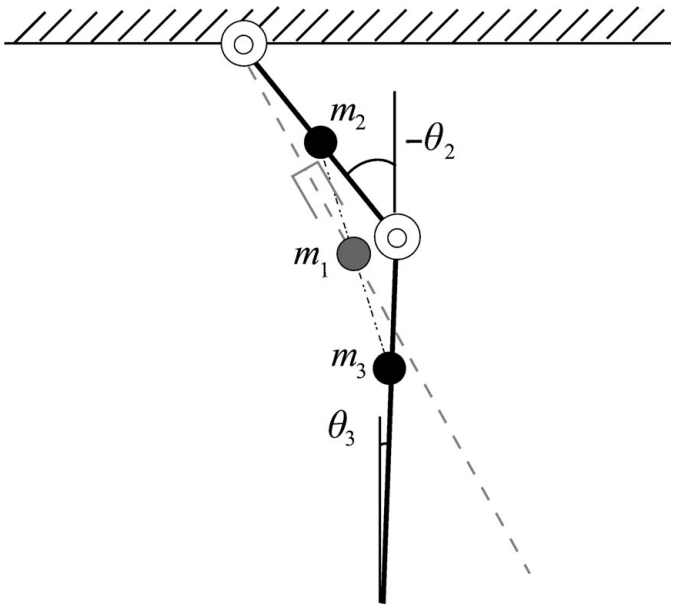

Fig. 5. Double pendulum and its equivalent one-link model with prismatic joint.

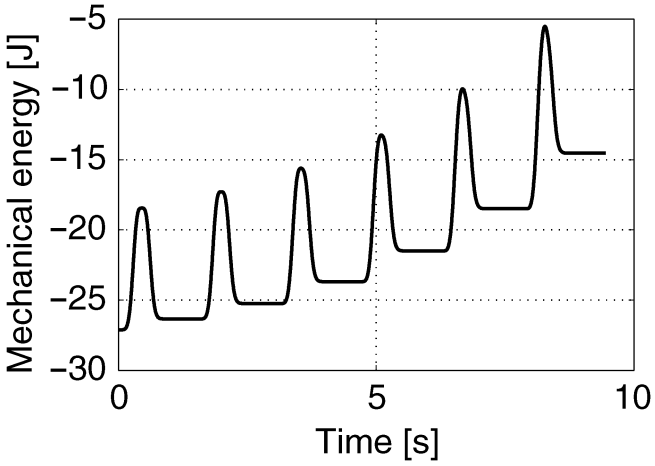

Fig. 6. Total mechanical energy of double pendulum.

dissipated in Fig. 7. This is because the relative angular velocity, $\dot{\theta}_2 - \dot{\theta}_3$, is almost zero at the collision. From this result, it is expected that a sustainable gait of biped robots with knees can be generated by this approach based on the parametric excitation principle.

5. Gait Generation on Rotary Actuation System Based on Parametric Excitation Principle

5.1. Control input design

In Section 4, we have shown that bending and stretching a knee increases energy for a double pendulum. It is expected that a sustainable gait can also be generated by parametric excitation for bending and stretching a knee. In this section, we propose a control design for a kneed biped robot shown in Fig. 1.

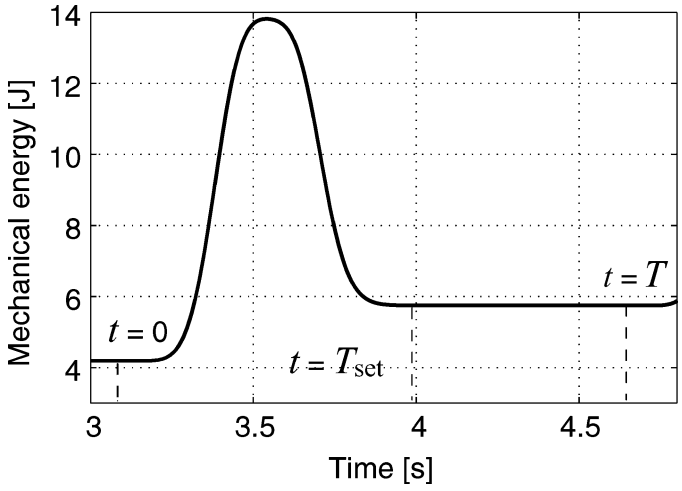

Fig. 7. Enlarged illustration of Fig. 6.

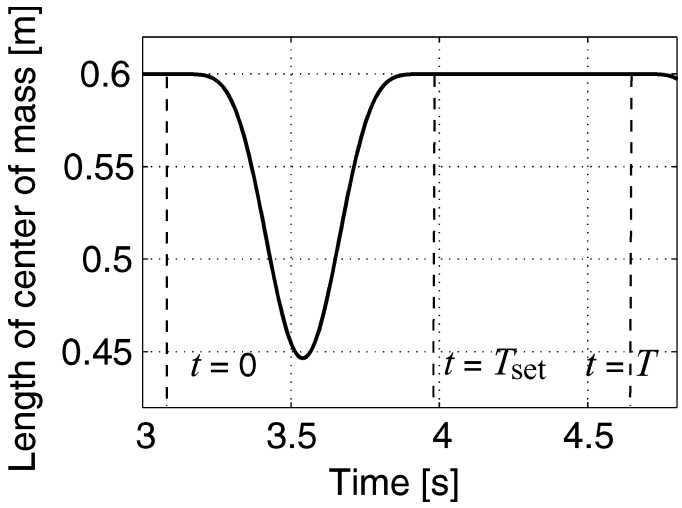

Fig. 8. Distance between support point and center of mass.

First, we explain the reference trajectory. We give the reference trajectory for the relative knee-joint angle as

$$(\theta_2 - \theta_3)_d = f(t) = \begin{cases} A_m \sin^3\left(\frac{\pi}{T_{set}-\delta}(t-\delta)\right) & (\delta \le t \le T_{\text{set}}), \\ 0 & (\text{otherwise}), \end{cases} \quad (4)$$

where $\delta > 0$ is the bending delay. Here, we suppose the instance just after the third phase as the initial time of the cycle, $t = 0$ s. The difference between Eq. (3) and Eq. (4) is the bending delay δ. We explain the reason why we introduce the bending delay by referring to Fig. 9. Figure 9 shows the reference trajectory, where a dashed-dotted line is the optimal trajectory for parametric excitation shown in Fig. 2, a dashed line is the case of $\delta = 0$ s with $T_{\text{set}} = 0.8$ s, a solid line is the case of $\delta = 0.2$ s with $T_{\text{set}} = 0.8$ s, and a dotted line is the case of $\delta = 0$ s with $T_{\text{set}} = 1.2$ s. In the reference trajectory of form (3), the trajectory shown by the dotted line is closest to the optimal trajectory when $T_{\text{set}} = 1.2$ s. However, in the case of a biped robot, a collision at the ground may occur before straightening the knee for this trajectory. To avoid this, we should make the reference trajectory close to the optimal

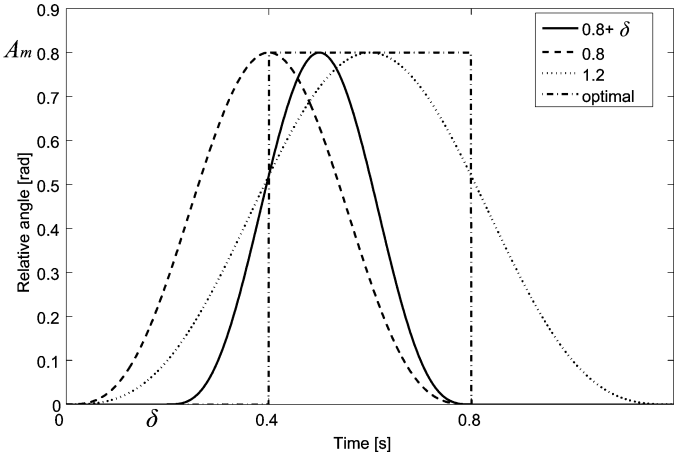

Fig. 9. Reference trajectory.

trajectory without increasing T_{set}. From Fig. 9, it is shown that by introducing bending delay δ, the reference trajectory approaches the optimal trajectory, and hence it is expected to restore more mechanical energy than those without delay.

Below we design a control input to track the reference trajectory given by Eq. (4). If we define $\boldsymbol{x} = [\theta_1\ \theta_2\ \theta_2 - \theta_3 - f\,]^{\mathrm{T}}$, then $\boldsymbol{\theta}$ is rewritten by

$$\boldsymbol{\theta} = \begin{bmatrix} 1 & 0 & 0 \\ 0 & 1 & 0 \\ 0 & 1 & -1 \end{bmatrix} \boldsymbol{x} + \begin{bmatrix} 0 \\ 0 \\ -1 \end{bmatrix} f =: \boldsymbol{L}\boldsymbol{x} + \boldsymbol{N} f, \tag{5}$$

and $\dot{\boldsymbol{\theta}}$ and $\ddot{\boldsymbol{\theta}}$ are

$$\dot{\boldsymbol{\theta}} = \boldsymbol{L}\dot{\boldsymbol{x}} + \boldsymbol{N}\dot{f}, \tag{6}$$

$$\ddot{\boldsymbol{\theta}} = \boldsymbol{L}\ddot{\boldsymbol{x}} + \boldsymbol{N}\ddot{f}, \tag{7}$$

respectively. The dynamic equation (1) is redefined as

$$\boldsymbol{M}\boldsymbol{L}\ddot{\boldsymbol{x}} + \boldsymbol{M}\boldsymbol{N}\ddot{f} + \boldsymbol{C}\boldsymbol{L}\dot{\boldsymbol{x}} + \boldsymbol{C}\boldsymbol{N}\dot{f} + \boldsymbol{g} = \boldsymbol{S}u_K. \tag{8}$$

Define K and Z as

$$\begin{aligned} K &= -\boldsymbol{N}^{\mathrm{T}}\boldsymbol{L}^{-1}\boldsymbol{M}^{-1}\boldsymbol{S}, \\ Z &= -\boldsymbol{N}^{\mathrm{T}}\boldsymbol{L}^{-1}\boldsymbol{M}^{-1}(\boldsymbol{M}\boldsymbol{N}\ddot{f} + \boldsymbol{C}\boldsymbol{L}\dot{\boldsymbol{x}} + \boldsymbol{C}\boldsymbol{N}\dot{f} + \boldsymbol{g}), \end{aligned} \tag{9}$$

and select the knee torque, u_K, as

$$u_K = K^{-1}Z. \tag{10}$$

Then, by using Eqs. (9) and (10) the dynamic equation (8) reduces to

$$\ddot{\theta}_2 - \ddot{\theta}_3 = \ddot{f}. \tag{11}$$

By integrating this equation twice, we obtain

$$\begin{aligned} &(\theta_2(t) - \theta_3(t)) - (\theta_2(0) - \theta_3(0)) - (\dot{\theta}_2(0) - \dot{\theta}_3(0))t \\ &\quad = f(t) - f(0) - \dot{f}(0)t. \end{aligned} \tag{12}$$

If initial states are set to equal initial states of the reference trajectory, i.e., $\dot{\theta}_2(0) - \dot{\theta}_3(0) = \dot{f}(0)$ and $\theta_2(0) - \theta_3(0) = f(0)$, then Eq. (12) reduces to

$$\theta_2(t) - \theta_3(t) = f(t). \tag{13}$$

Therefore, $\theta_2 - \theta_3$ corresponds with the reference trajectory by the input u_K given by Eq. (10).

5.2. Numerical simulation

Parameters of the biped robot are shown in Table I. The parameters of the reference trajectory are set as $A_m = 1.2$ rad, $T_{\text{set}} = 0.8$ s, and $\delta = 0.2$ s.

Simulation results of parametric excitation based walking by knee-joint actuation are shown in Fig. 10 which illustrates about three steps from 105 to 108 s after starting to walk. Simulation results show that a sustainable gait can be generated without a hip torque. Figure 10(a) shows angular positions, 10(b) shows angular velocities, 10(c) shows the total mechanical energy, 10(d) shows knee torque, u_K, 10(e) shows foot clearance, 10(f) shows distance between the hip joint and the center of mass of the swing-leg, and 10(g) shows knee-joint angle, i.e., $\theta_2 - \theta_3$. From Figs. 10(c) and 10(f), it is observed that the total mechanical energy increases when a knee of a biped robot is bended and that the total energy decreases when a knee is stretched. This is because potential energy increases with knee bending and decreases with knee stretching. The difference between the energy increase and the energy decrease is the quantity of total energy restoration. From Fig. 10(c), it can be observed that energy dissipation of the collision at the knee is almost negligible because relative angular velocity equals almost zero just before the knee impact. In our approach we expected to avoid scuffing the ground similarly like a biped robot with telescopic-legs. It is observed from Fig. 10(e) that this biped robot avoids scuffing the ground. Figure 11 shows a stick diagram of parametric excited based walking for a kneed biped robot. In this figure, the dashed lines are support-legs and the solid lines are swing-legs.

6. Effect of Parameters

In this section, we examine the influences of the ratio of lengths between upper leg and lower leg to foot clearance. We also examine the effect of parameters of the reference trajectory for walking efficiency. To do these, we simulate the cases of foot radii, $R = 0.45$, 0.50, and 0.55 m.

6.1. Effect of length between upper leg and lower leg

We first examine the effect of length between upper leg, a_2, and lower leg, a_3, for foot clearance. We fix $a_2 + a_3 = 1.0$ m and simulate numerically by changing the ratio.

We show simulation results in Fig. 12. Parameters of a biped robot are the same as those in the preceding section except for a_2, a_3, r_2, r_3, and the parameters of the reference trajectory are set as follows: $A_m = 1.2$ rad, $T_{\text{set}} = 0.8$ s, and $\delta = 0.2$ s. The length of upper leg, a_2, is changed from 0.3 to 0.55m. The centers of mass of each link are as follows: $r_2 = a_2/2$, $r_3 = a_3/2$. We show the results of only those bipedal walking convergences.

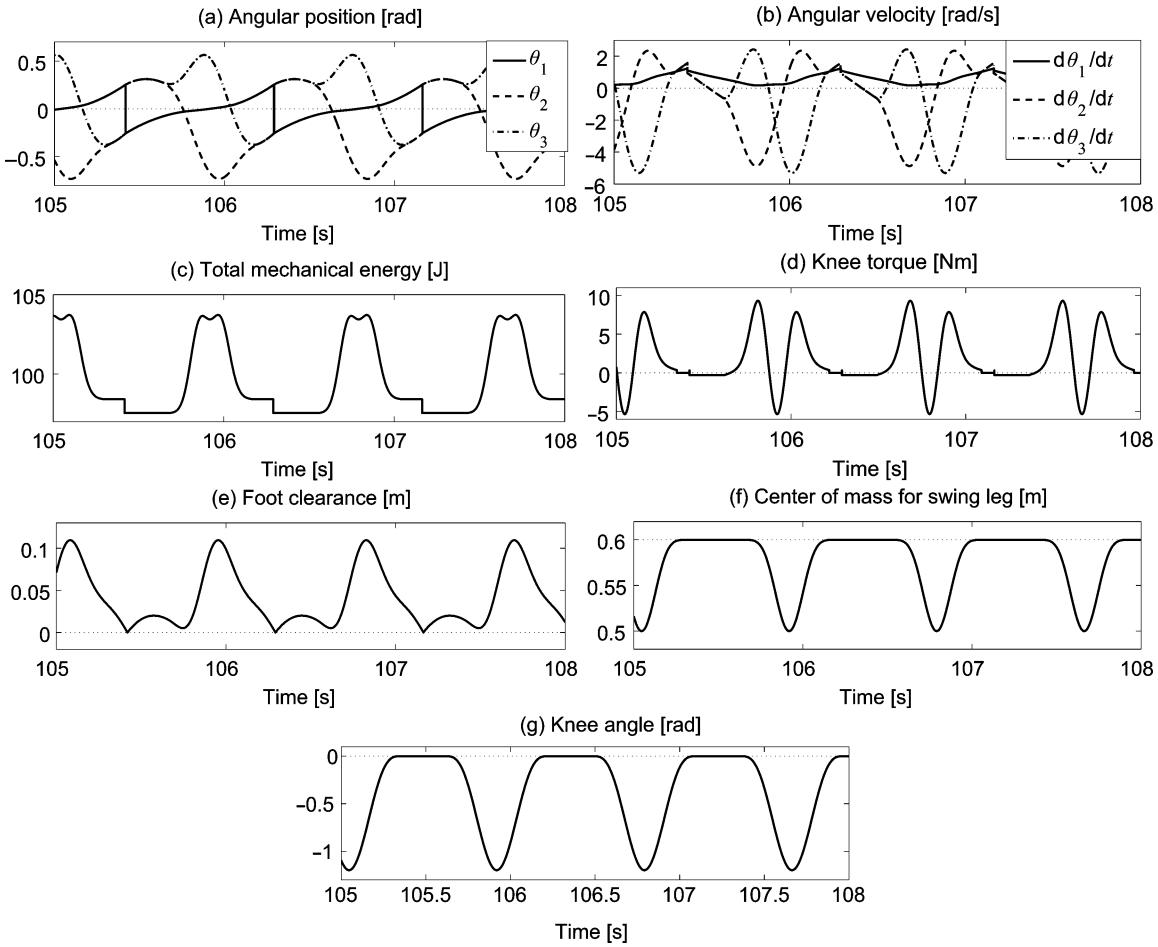

Fig. 10. Simulation results for steady gait pattern.

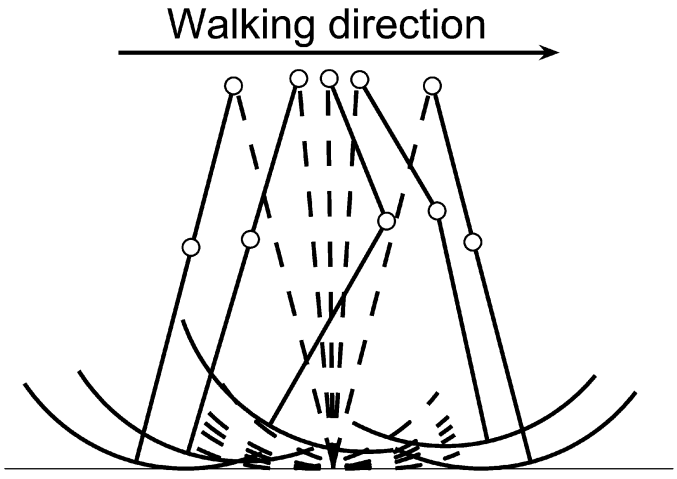

Fig. 11. Stick diagram for steady gait pattern.

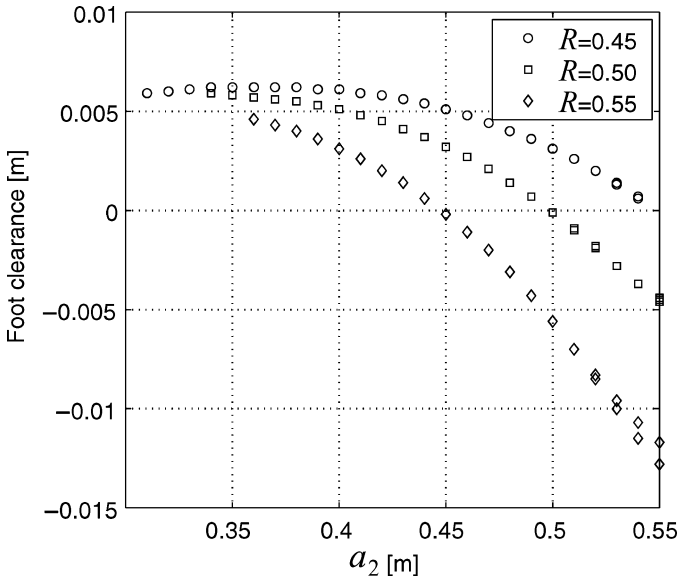

Fig. 12. Foot clearance with respect to a_2.

In Fig. 12, circles represent the results of foot radius $R = 0.45$ m, squares the results of $R = 0.50$ m, and diamonds the results of $R = 0.55$ m. In the case of $R = 0.45$ m, we show results for a_2 from 0.31 to 0.54 m; in the case of $R = 0.50$ m, we show results for a_2 from 0.34 to 0.55 m; and in the case of $R = 0.55$ m, we show results for a_2 from 0.36 to 0.55 m.

From Fig. 12, we may observe that the smaller the a_2, the larger is the foot clearance. For the same ratio, a large foot is bad for foot clearance. It is also observed that bifurcation occurs when a_2 is beyond 0.48 m in the case of $R = 0.45$ m, a_2 is beyond 0.48 m in the case of $R = 0.50$ m, and a_2 is beyond 0.49 m in the case of $R = 0.55$ m.

6.2. *Effect of reference trajectory*

In this subsection, we examine the effect of the reference trajectory on some walking indices such as step period,

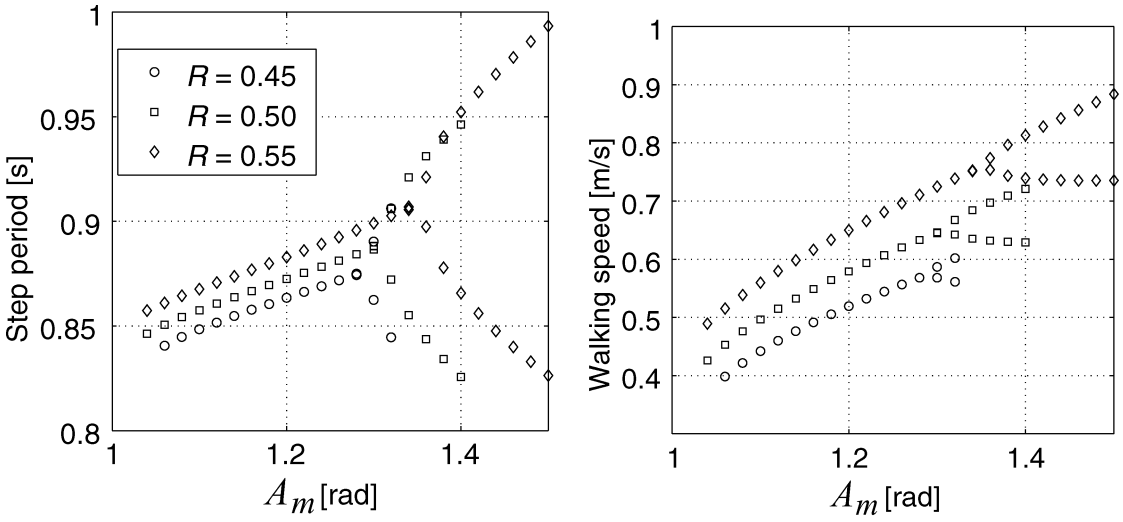

(a) Step period

(b) Walking speed

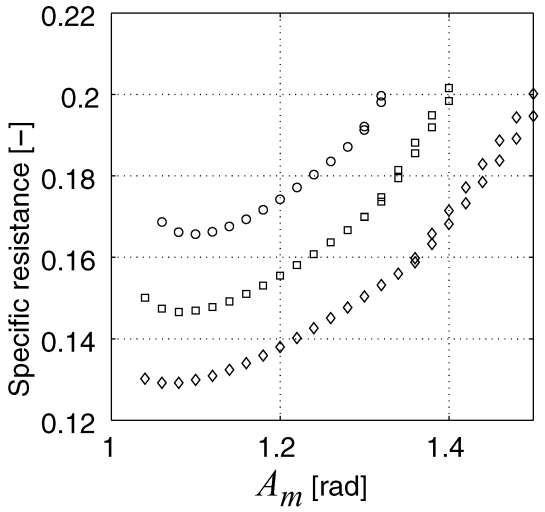

(c) Specific resistance

Fig. 13. Gait descriptors with respect to A_m.

walking speed, and specific resistance. The specific resistance defined by

$$\mu = \frac{\int_{0^+}^{T^-} |u_K(\dot{\theta}_2 - \dot{\theta}_3)| \mathrm{d}t / T}{M_g g \overline{V}} \tag{14}$$

represents energy efficiency, and walking is more efficient as this value is smaller. In Eq. (14), 0^+ and T^- represent the time just after and before collision at the ground, respectively, M_g is the total mass of a biped robot, and $\overline{V}$ is the average walking speed. We note that, in the simulation of this subsection, the problem of foot clearance is not taken into consideration, that is, we regard that a biped robot walks sustainably even if a foot scuffs the ground.

First, we show the simulation results when we fix $T_{\mathrm{set}} = 0.8$ s and $\delta = 0.2$ s and when we change the amplitude of vibration, A_m, from 1.0 to 1.5 rad. We show the results of only those bipedal walking convergences. Figure 13(a) shows the step period, 13(b) shows the walking speed, and 13(c) shows the specific resistance. In the case of $R = 0.45$ m, results are shown for A_m from 1.04 to 1.4 rad; in the case of $R = 0.50$ m, results are shown for A_m from 1.02 to 1.44 rad; and in the case of $R = 0.55$ m, results are shown for A_m from 1.04 to 1.5 rad. The figure shows that the larger the amplitude of vibration, A_m, is, the larger are the step period and the walking speed. On the other hand, specific resistance first becomes smaller and then larger as A_m increases. Therefore, in the case of $R = 0.45$ m, walking is most efficient when $A_m = 1.1$ rad; in the case of $R = 0.50$ m, walking is most efficient when $A_m = 1.1$ rad; and in the case of $R = 0.55$ m, walking is most efficient when $A_m = 1.08$ rad. For the same amplitude of vibration, A_m, the walking speed becomes large and the specific resistance becomes small when the foot radius is large. In addition, bifurcation occurs when A_m becomes large.

Next, we show the simulation results of changing delay, δ. In this simulation, we fix $T_{\mathrm{set}} = 0.8$ s and $A_m = 1.2$ rad

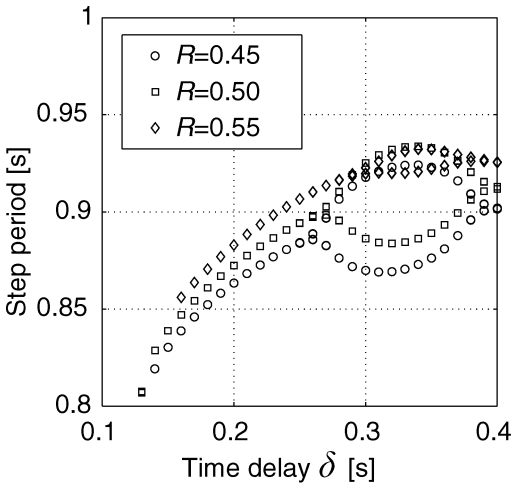

(a) Step period

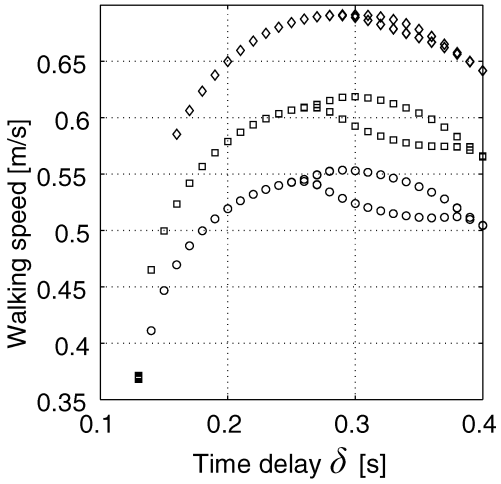

(b) Walking speed

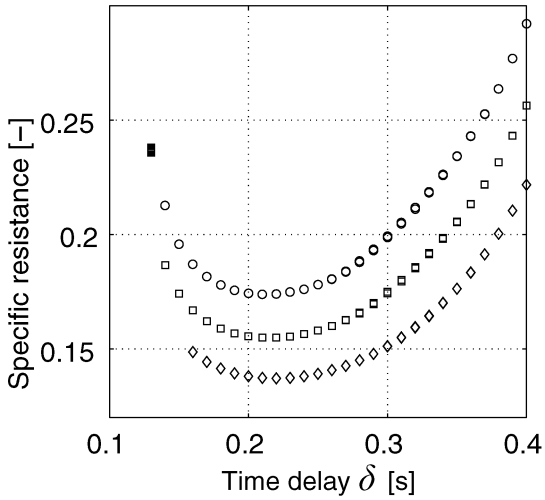

(c) Specific resistance

Fig. 14. Gait descriptors with respect to δ.

and δ is changed from 0.05 to 0.40 s. Figure 14(a) shows the step period, 14(b) the walking speed, and 14(c) the specific resistance. In the case of $R = 0.45$ m, results are shown for δ from 0.13 to 0.40 s; in the case of $R = 0.50$ m, results are shown for δ from 0.14 to 0.40 s; and in the case of $R = 0.55$ m, results are shown for δ from 0.16 to 0.40 s. We show the results for only those bipedal walking convergences. The figure shows that the larger the delay, δ, is, the larger are the step period and the walking speed. On the other hand, specific resistance first becomes smaller and then larger as δ increases. Therefore, in the case of $R = 0.45$ m, walking is most efficient when $\delta = 0.21$ s; in the case of $R = 0.50$ m, walking is most efficient when $\delta = 0.22$ s; and in the case of $R = 0.55$ m, walking is most efficient when $\delta = 0.22$ s. This is because the reference trajectory is closest to the optimal trajectory when $\delta = 0.22$ s as shown in Fig. 9. For the same delay, δ, the walking speed becomes large and specific resistance becomes small when the foot radius is large. It is also observed that bifurcation occurs when δ becomes large. We note that the biped robot scuffs the ground in the range of large bending delays, such as larger than 0.33 s.

From these results, we can see that a large foot has advantages with respect to walking speed and energy efficiency. On the other hand, a large foot is bad for foot clearance. There is trade-off between efficiency and foot clearance. Because of this we have adopted the length of the upper leg, $a_2 = 0.4$ m, and the foot radius, $R = 0.5$m, in the simulation of Section 5.

6.3. Basin of attraction

In this subsection, we analyze the basin of attraction with respect to the initial conditions. To do this, we consider a certain sustainable gait for which the target control input corresponds to $A_m = 1.2$ rad, $T_{\text{set}} = 0.8$ s, $\delta = 0.2$ s, and then we simulate the motion in the several initial conditions. Our robot has three degrees of freedom for initial conditions, i.e., support-leg angle, support-leg angular velocity, and swing-leg angular velocity. In the case of changing the swing-leg

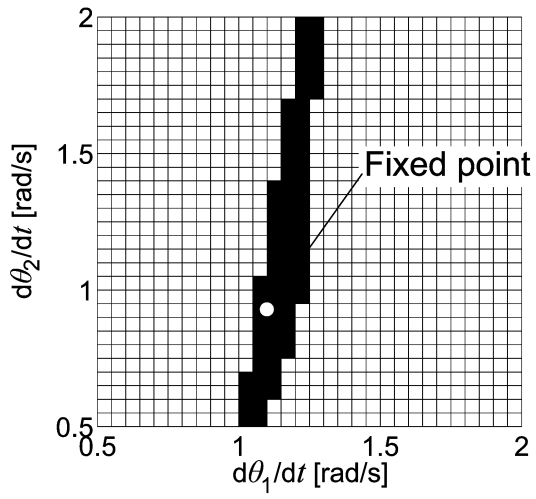

(a) Attraction with fixed θ_1

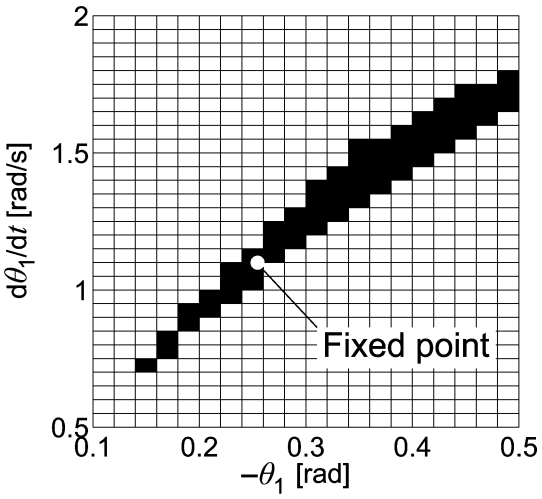

(b) Attraction with fixed $\dot{\theta}_2$

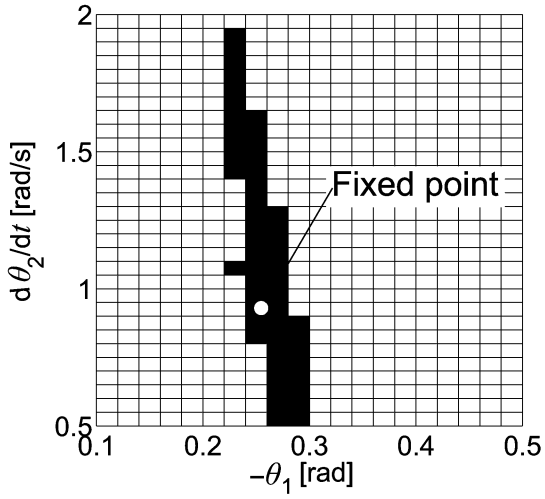

(c) Attraction with fixed $\dot{\theta}_1$

Fig. 15. Basin of attraction.

angle, we change the angle from 0.0 to 0.4 rad. In the cases of changing the angular velocity, we change the angular velocity from 0.0 to 3.0 rad/s. The initial conditions belong to the basin of attraction when the biped robot walks 200 steps successfully. In this simulation, we also ignore the problem of foot clearance as in the previous subsection.

Simulation results of the basin of attraction are shown in Fig. 15. The axes represent the initial state of the system. Simulations have been performed on three-dimensional spaces of parameters, but we depict three slices of two-dimensional figures for the purpose of visibility. Figure 15(a) shows the slice of the results at θ_1 fixed to -0.2548 rad, 15(b) shows that of $\dot{\theta}_2 = 0.9299$ rad/s, and 15(c) shows that of $\dot{\theta}_1 = 1.0992$ rad/s. In these figures, the black regions indicate the initial conditions from which the robot walks sustainably and the initial condition converges to the fixed point indicated by the white circle, $[\theta_1\ \theta_2\ \theta_3\ \dot{\theta}_1\ \dot{\theta}_2\ \dot{\theta}_3\ ] = [-0.2548\ 0.2548\ 0.2548\ 1.0992\ 0.9299\ 0.9299\ ]$. From the figures, it is observed that the maximum radius of the ball, which is contained in the basin of attraction, centered at the fixed point is 5.38% in relative error.

7. Conclusion and Future Work

In this paper, we applied the parametric excitation principle to a kneed biped robot, and showed that only knee actuation generated sustainable gait. In particular, we resolved the problem of foot clearance by revising the ratio of thigh and shin lengths. We optimized the reference trajectory by introducing bending delay. In addition, we showed the effect of parameters on efficiency and showed the basin of attraction.

In future work, we will search the optimal robot parameters and the optimal reference trajectory. We will also combine the hip torque with the knee torque and generate more efficient bipedal walking, and we will apply this method to a real machine. We guess that energy restoration based on parametric excitation is not only realized by bending and

stretching the swing-leg but also by using the support-leg, torso, and arms. It should be investigated that the method generates a sustainable gait by using the support-leg, torso, and arm motion. In addition, we conjecture that the center of mass of a human being moves up and down while walking and hence this motion restores the total mechanical energy based on the parametric excitation principle. It is also an important research issue to measure the human walking motion and analyze the motion to verify whether human walking makes use of the parametric excitation principle or not.

References

1. T. McGeer, "Passive dynamic walking," *Int. J. Robot. Res.* **9**(2), 62–82 (1990).
2. F. Asano, M. Yamakita and K. Furuta, "Virtual passive dynamic walking and energy-based control laws," *IEEE/RSJ International Conference on Intelligent Robotics and Systems*, vol. 2 (2000), pp. 1149–1154.
3. A. Goswami, B. Espiau and A. Keramane, "Limit cycles in a passive compass gait biped and passivity-mimicking control laws," *J. Autonom. Robots* **4**(3), 273–286 (1997).
4. F. Asano, Z. W. Luo and S. Hyon, "Parametric excitation mechanisms for dynamic bipedal walking," *IEEE International Conference on Robotics and Automation* (2005) pp. 611–617.
5. F. Asano, T. Hayashi, Z. W. Luo, S. Hirano and A. Kato, "Parametric excitation approaches to efficient bipedal walking," *Proceedings of the 2007 IEEE/RSJ International Conference on Intelligent Robots and Systems* (2007) pp. 2210–2216.
6. Y. Harata, F. Asano, Z. W. Luo, K. Taji and Y. Uno, "Biped gait generation based on parametric excitation by knee-joint actuation," *Proceedings of the 2007 IEEE/RSJ International Conference on Intelligent Robots and Systems* (2007) pp. 2198–2203.
7. E. K. Lavrovskii and A. M. Formalskii, "Optimal control of the pumping and damping of swing," *J. Appl. Math. Mech.* **57**(2), 311–320 (1993).

Appendix A: Dynamic Equation

Each element, $\boldsymbol{M}$, $\boldsymbol{C}$, and $\boldsymbol{g}$, of dynamic equation (1) of a biped robot shown in Fig. 1 is given by

$$
\begin{aligned}
M_{11}(\boldsymbol{\theta}) &= m_1(R^2 + (r_1 - R)^2) + 2m_1R(r_1 - R)\cos\theta_1 \\
&\quad + (m_H + m_2 + m_3)((R^2 + (l - R)^2) \\
&\quad + 2R(l - R)\cos\theta_1) + I \\
M_{12}(\boldsymbol{\theta}) &= -(m_2r_2 + m_3a_2)(l - R)\cos(\theta_1 - \theta_2) \\
&\quad - (m_2r_2 + m_3a_2)R\cos\theta_2 \\
M_{13}(\boldsymbol{\theta}) &= -m_3r_3(l - R)\cos(\theta_1 - \theta_3) - m_3Rr_3\cos\theta_3 \\
M_{21}(\boldsymbol{\theta}) &= M_{12}(\boldsymbol{\theta}) \\
M_{22}(\boldsymbol{\theta}) &= m_2r_2^2 + m_3a_2^2 \\
M_{23}(\boldsymbol{\theta}) &= m_3a_2r_3\cos(\theta_2 - \theta_3) \\
M_{31}(\boldsymbol{\theta}) &= M_{13}(\boldsymbol{\theta}) \\
M_{32}(\boldsymbol{\theta}) &= M_{23}(\boldsymbol{\theta}) \\
M_{33}(\boldsymbol{\theta}) &= m_3r_3^2 \\
C_{11}(\boldsymbol{\theta}, \dot{\boldsymbol{\theta}}) &= (-m_1R(r_1 - R) - (m_H + m_2 + m_3) \\
&\quad R(l - R))\dot{\theta}_1\sin\theta_1 \\
C_{12}(\boldsymbol{\theta}, \dot{\boldsymbol{\theta}}) &= (m_2r_2 + m_3a_2)(-(l - R)\sin(\theta_1 - \theta_2) \\
&\quad + R\sin\theta_2)\dot{\theta}_2 \\
C_{13}(\boldsymbol{\theta}, \dot{\boldsymbol{\theta}}) &= (-m_3r_3(l - R)\sin(\theta_1 - \theta_3) + m_3Rr_3\sin\theta_3) \\
&\quad \dot{\theta}_3 \\
C_{21}(\boldsymbol{\theta}, \dot{\boldsymbol{\theta}}) &= (m_2r_2 + m_3a_2)(l - R)\sin(\theta_1 - \theta_2)\dot{\theta}_1 \\
C_{22}(\boldsymbol{\theta}, \dot{\boldsymbol{\theta}}) &= 0 \\
C_{23}(\boldsymbol{\theta}, \dot{\boldsymbol{\theta}}) &= m_3a_2r_3\sin(\theta_2 - \theta_3)\dot{\theta}_3 \\
C_{31}(\boldsymbol{\theta}, \dot{\boldsymbol{\theta}}) &= m_3(l - R)r_3\sin(\theta_1 - \theta_3)\dot{\theta}_1 \\
C_{32}(\boldsymbol{\theta}, \dot{\boldsymbol{\theta}}) &= -m_3a_2r_3\sin(\theta_2 - \theta_3)\dot{\theta}_2 \\
C_{33}(\boldsymbol{\theta}, \dot{\boldsymbol{\theta}}) &= 0 \\
g_1(\boldsymbol{\theta}) &= -g(m_1(r_1 - R) + (m_H + m_2 + m_3)(l - R)) \\
&\quad \sin\theta_1 \\
g_2(\boldsymbol{\theta}) &= g(m_2r_2 + m_3a_2)\sin\theta_2 \\
g_3(\boldsymbol{\theta}) &= gm_3r_3\sin\theta_3
\end{aligned}
$$

Matrix $\boldsymbol{S}$ is given by

$$
\boldsymbol{S} = \begin{bmatrix} 0 \\ -1 \\ 1 \end{bmatrix}. \tag{15}
$$

Appendix B: Impact Equations

B.1. Impact equation at knee

In the biped robot model dealt with in this paper, there are collisions at the knee and the ground. First, we explain an impact equation at the knee. When a swing-leg straightens, a completely inelastic collision is assumed to occur at a knee of the swing-leg. The coordinates $\dot{\boldsymbol{\theta}}^-$ and $\dot{\boldsymbol{\theta}}^+$, which correspond to before and after knee impact, respectively, are related by the following equation:

$$
\boldsymbol{M}\dot{\boldsymbol{\theta}}^+ = \boldsymbol{M}\dot{\boldsymbol{\theta}}^- + \boldsymbol{J}^{\mathrm{T}}\lambda_I, \tag{16}
$$

where λ_I is constraint force making $\boldsymbol{J}\dot{\boldsymbol{\theta}}^+ = 0$. This force is given by

$$
\lambda_I = -(\boldsymbol{J}\boldsymbol{M}^{-1}\boldsymbol{J}^{\mathrm{T}})^{-1}\boldsymbol{J}\dot{\boldsymbol{\theta}}^-. \tag{17}
$$

From Eqs. (16) and (17), angular velocities after knee impact are given by

$$
\dot{\boldsymbol{\theta}}^+ = -(\boldsymbol{I} - \boldsymbol{M}^{-1}\boldsymbol{J}^{\mathrm{T}}(\boldsymbol{J}\boldsymbol{M}^{-1}\boldsymbol{J}^{\mathrm{T}})^{-1}\boldsymbol{J})\dot{\boldsymbol{\theta}}^-. \tag{18}
$$

On the other hand, we have $\boldsymbol{\theta}^- = \boldsymbol{\theta}^+$, because angular positions do not change before and after the impact.

B.2. Impact equation at ground

Next, we explain impact equation at the ground. A completely inelastic collision is assumed to occur at the ground. Extended generalized coordinate for separated legs i ($i = 1, 2$) shown in Fig. 16 is given by

$$
\boldsymbol{q} = \begin{bmatrix} \boldsymbol{q}_1 \\ \boldsymbol{q}_2 \end{bmatrix}, \tag{19}
$$

where $\boldsymbol{q}_i = [x_i\ z_i\ \theta_{i1}\ \theta_{i2}]^{\mathrm{T}}$. Let "$-$" and "$+$" be superscripts corresponding to before and after impact at the ground, respectively. Then, we have $\boldsymbol{\theta}^- = \boldsymbol{\theta}^+$, because positions do

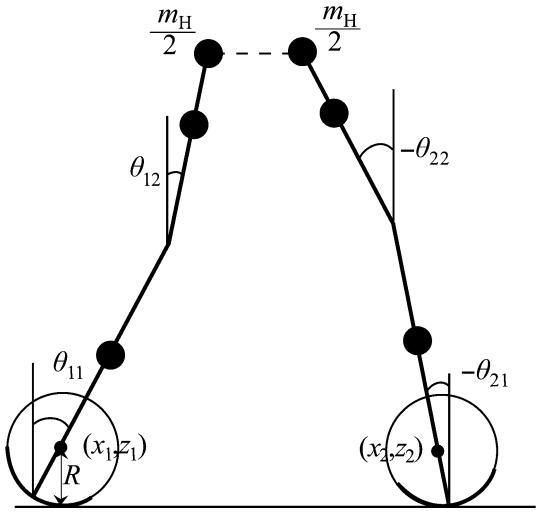

Fig. 16. Geometric relation at the heel-strike instant.

not change before and after the impact. Impact equation of extended generalized coordinate is given by

$$\bar{\boldsymbol{M}}(\boldsymbol{q})\dot{\boldsymbol{q}}^{+} = \bar{\boldsymbol{M}}(\boldsymbol{q})\dot{\boldsymbol{q}}^{-} - \boldsymbol{J}_I(\boldsymbol{q})^{\mathrm{T}}\boldsymbol{\lambda}_I, \tag{20}$$

where $\boldsymbol{\lambda}_I \in \mathbb{R}^6$ is an undetermined multiplier vector which is impulse force. $\bar{\boldsymbol{M}}(\boldsymbol{q}) \in \mathbb{R}^{8\times 8}$ is the inertia matrix given by

$$\bar{\boldsymbol{M}}(\boldsymbol{q}) = \begin{bmatrix} \tilde{\boldsymbol{M}}^1(\boldsymbol{q}_1) & \boldsymbol{0}_{4\times 4} \\ \boldsymbol{0}_{4\times 4} & \tilde{\boldsymbol{M}}^2(\boldsymbol{q}_2) \end{bmatrix}. \tag{21}$$

$\tilde{\boldsymbol{M}}^i$ $(i = 1, 2)$ are given by

$$\begin{aligned}
\tilde{\boldsymbol{M}}^i_{11} &= m_2 + m_3 + m_H/2 \\
\tilde{\boldsymbol{M}}^i_{12} &= 0 \\
\tilde{\boldsymbol{M}}^i_{13} &= (m_3(a_3 - r_3 - R) + (m_2 + m_H/2)(a_3 - R)) \\
&\quad \cos\,\theta_{i1} \\
\tilde{\boldsymbol{M}}^i_{14} &= (m_2(a_2 - r_2) + m_H a_2/2)\cos\theta_{i2} \\
\tilde{\boldsymbol{M}}^i_{21} &= 0 \\
\tilde{\boldsymbol{M}}^i_{22} &= m_2 + m_3 + m_H/2 \\
\tilde{\boldsymbol{M}}^i_{23} &= -(m_3(a_3 - r_3 - R) + (m_2 + m_H/2)(a_3 - R) \\
&\quad \sin\,\theta_{i1} \\
\tilde{\boldsymbol{M}}^i_{24} &= -(m_2(a_2 - r_2) + m_H a_2/2)\sin\theta_{i2} \\
\tilde{\boldsymbol{M}}^i_{31} &= \tilde{\boldsymbol{M}}^i_{13} \\
\tilde{\boldsymbol{M}}^i_{32} &= \tilde{\boldsymbol{M}}^i_{23} \\
\tilde{\boldsymbol{M}}^i_{33} &= m_3(a_3 - r_3 - R)^2 + (m_2 + m_H/2)(a_3 - R)^2 \\
\tilde{\boldsymbol{M}}^i_{34} &= (m_2(a_2 - r_2) + m_H a_2/2)\cos\theta_{i2} \\
\tilde{\boldsymbol{M}}^i_{41} &= \tilde{\boldsymbol{M}}^i_{14} \\
\tilde{\boldsymbol{M}}^i_{42} &= \tilde{\boldsymbol{M}}^i_{24} \\
\tilde{\boldsymbol{M}}^i_{43} &= \tilde{\boldsymbol{M}}^i_{34} \\
\tilde{\boldsymbol{M}}^i_{44} &= m_2(a_2 - r_2)^2 + m_H a_2^2/2.
\end{aligned}$$

$\boldsymbol{J}_I \in \mathbb{R}^{6\times 8}$ is the Jacobian which satisfies the condition

$$\boldsymbol{J}_I(\boldsymbol{q})\dot{\boldsymbol{q}}^{+} = \boldsymbol{0}_{6\times 1}. \tag{22}$$

There are some constraints among coordinates. First, from geometric conditions we have

$$\begin{aligned}
z_2 &= R, \\
& x_1 + (a_3 - R)\sin\theta_{11} + a_2\sin\theta_{12} \\
&= x_2 + (a_3 - R)\sin\theta_{21} + a_2\sin\theta_{22,} \\
& z_1 + (a_1 - R)\cos\theta_{11} + a_2\cos\theta_{12} \\
&= z_2 + (a_1 - R)cos\theta_{21} + a_2\cos\theta_{22}.
\end{aligned} \tag{23}$$

These equations mean that the height of the center of foot of the support-leg is constant (equal to foot radius) and that the hip position (vertical and horizontal) from (x_1, z_1) equals to the hip position from (x_2, z_2). In addition, the rate constraint that the foot of the support-leg rolls on the ground is given by

$$\dot{x}_2^{+} = R\dot{\theta}_{21}^{+}. \tag{24}$$

The rate constraints that knees are stretched are given by

$$\begin{aligned}
\dot{\theta}_{11}^{+} &= \dot{\theta}_{12,}^{+} \\
\dot{\theta}_{21}^{+} &= \dot{\theta}_{22}^{+}.
\end{aligned} \tag{25}$$

$\boldsymbol{J}_I$ is derived from differentiating Eq. (23) and by incorporating Eqs. (24) and (25).

The multiplier vector $\boldsymbol{\lambda}_I$ is given by

$$\boldsymbol{\lambda}_I = \boldsymbol{X}_I^{-1}\boldsymbol{J}_I\dot{\boldsymbol{q}}^{-}, \tag{26}$$

where matrix $\boldsymbol{X}_I$ is given by

$$\boldsymbol{X}_I = \boldsymbol{J}_I\bar{\boldsymbol{M}}^{-1}\boldsymbol{J}_I^{\mathrm{T}}. \tag{27}$$

As above, velocity of the extended generalized coordinate after collision is given by

$$\dot{\boldsymbol{q}}^{+} = \left(\boldsymbol{I}_8 - \bar{\boldsymbol{M}}^{-1}\boldsymbol{J}_I^{\mathrm{T}}\boldsymbol{X}_I^{-1}\boldsymbol{J}_I\right)\dot{\boldsymbol{q}}^{-}. \tag{28}$$